

Optimal User and Target Scheduling, User-Target Pairing, and Low-Resolution Phase-Only Beamforming for ISAC Systems

Luis F. Abanto-Leon and Setareh Maghsudi

Abstract—We investigate the joint user and target scheduling, user-target pairing, and low-resolution phase-only beamforming design for integrated sensing and communications (ISAC). Scheduling determines which users and targets are served, while pairing specifies which users and targets are grouped into pairs. Additionally, the beamformers are designed using few-bit constant-modulus phase shifts. This resource allocation problem is a nonconvex mixed-integer nonlinear program (MINLP) and challenging to solve. To address it, we propose an exact mixed-integer linear program (MILP) reformulation, which leads to a globally optimal solution. Our results demonstrate the superiority of an optimal joint design compared to heuristic stage-wise approaches, which are highly sensitive to scenario characteristics.

Index Terms—ISAC, sensing and communications, resource allocation, beamforming, discrete phases, scheduling, pairing.

I. INTRODUCTION

Integrated sensing and communications (ISAC) is an innovative technology offering several advantages, including improved radio resource utilization, reduced costs, and simplified system complexity [1]. However, ISAC also introduces new challenges, particularly in designing the radio resource allocation to jointly fulfill users' and targets' requirements.

To enhance sensing accuracy, recent ISAC literature has focused on high frequencies, such as millimeter-wave and terahertz bands, using beamforming to mitigate the severe path loss [2]. However, the high costs of radio components for controlling signals' amplitude and phase at these frequencies have led to the adoption of phase-only beamformers as a more cost-effective solution [3]. Despite the need for practical solutions, the literature primarily features designs with infinite-resolution phases, e.g., [4]–[7], which are infeasible in real-world deployments. Only a few works have accounted for low-resolution phases, e.g., [8], [9], but these designs have relied on approximations to handle phase discretization resulting in inefficient radio resource utilization and highlighting the need for novel approaches that can achieve an optimal design.

Practical systems often cannot simultaneously serve all users in a system due to limitations, e.g., in the number of radio-frequency (RF) chains, underscoring the need for user scheduling. While this aspect has been well investigated in communication systems, e.g., [10], yielding substantial gains, it remains unexplored in ISAC. Hence, incorporating user scheduling into ISAC's resource allocation could significantly

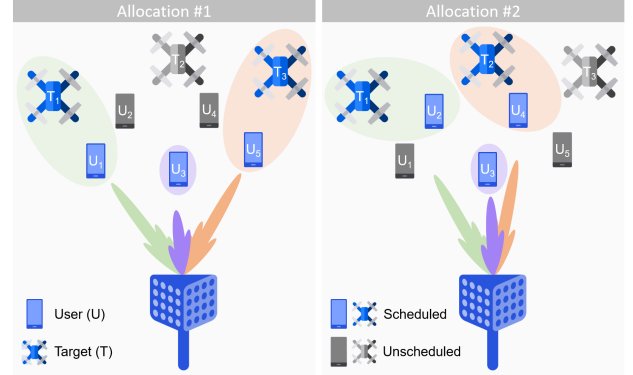


Fig. 1. ISAC system consisting of a BS and multiple users and targets. “Allocation #1” shows a favorable resource allocation strategy, featuring well-separated pairs and strong alignment between users and targets within each pair. This ensures high directivity, benefiting both users and targets. The sufficient spacing between scheduled users (U_1 , U_3 , U_5) minimizes inter-user interference, while the adequate separation between targets (T_1 , T_3) reduces cross-interference. In contrast, “Allocation #2” is less optimal due to closer pairs spread over a wider angular range, resulting in weaker alignment and reduced directivity. The angular proximity of users (U_2 , U_3 , U_4) increases inter-user interference, and the limited separation between targets (T_1 , T_2) heightens cross-correlation. While this scenario highlights the importance of alignment, a more comprehensive resource allocation approach is needed. Factors such as user channel conditions, target characteristics, and phase resolution significantly influence performance, necessitating a unified optimization strategy beyond fixed pairing and scheduling criteria.

enhance system performance by enabling optimized decision-making on which users to serve jointly.

Target scheduling is equally critical, aiming to optimize target selection for sensing while considering resource limitations. While a few studies, e.g., [11], have delved into this topic, it remains largely under-explored.

Most ISAC works have assumed that user-target pairing is predetermined and provided as prior information, e.g., [5], [6], [12], which is employed for subsequent resource allocation. Recently, however, there has been a shift towards exploring flexible user-target pairing, e.g., [13], [14], allowing for improved performance by dynamically associating users and targets based on factors such as location and channel conditions. Yet, existing studies on this topic have only considered one user per time slot, e.g., [13], [14], thereby avoiding multiuser interference. Exploiting spatial multiplexing to service multiple users and targets simultaneously is crucial in modern radar and communication systems, as it improves radio resource utilization, making it a key aspect to consider.

Jointly designing scheduling, pairing, and beamforming is a challenging task. Although performing these processes in separate stages can simplify the design, this decoupling often results in suboptimal performance. Particularly, pairing based on a single criterion, such as alignment, as shown

Copyright (c) 2025 IEEE. Personal use of this material is permitted. However, permission to use this material for any other purposes must be obtained from the IEEE by sending a request to pubs-permissions@ieee.org.

The authors are affiliated with Ruhr University Bochum, Germany.

The research was supported by the German Federal Ministry of Education and Research under projects 16KISK035 and 16KISK037.

in Fig. 1, is a valid approach. However, pairing cannot be treated in isolation from scheduling, as both are influenced by users' channel characteristics and targets' features. Furthermore, phase resolution constrains the beamforming directions, further emphasizing the interdependence between scheduling, pairing, and beamforming. This paper investigates the optimal joint design of these three key processes, resulting in a novel resource allocation problem that is formulated as a nonconvex mixed-integer nonlinear program (MINLP). We propose a reformulation that transforms the nonconvex MINLP into a mixed-integer linear program (MILP), enabling global optimality through convex transformations that preserve the original solution space. Simulations demonstrate that our joint design provides significant performance gains over four baseline methods inspired by existing literature, which rely on heuristic scheduling and pairing.

Notation: Matrices and vectors are respectively denoted by \mathbf{A} and \mathbf{a} . The transpose, Hermitian transpose, and trace of \mathbf{A} are denoted by \mathbf{A}^T , \mathbf{A}^H , and $\text{Tr}(\mathbf{A})$, respectively. The l -th row and i -th column of \mathbf{A} are denoted by $[\mathbf{A}]_{l,:}$ and $[\mathbf{A}]_{:,i}$, respectively, and the l -th element of \mathbf{a} is denoted by $[\mathbf{a}]_l$.

II. SYSTEM MODEL AND PROBLEM FORMULATION

We consider a multi-user, multi-target downlink ISAC system, as illustrated in Fig. 1, where the base station (BS) jointly performs sensing and communication tasks.

Preliminaries: The BS has N transmit antennas and N receive antennas, indexed by set $\mathcal{N} = \{1, \dots, N\}$. Also, there are T targets and U single-antenna users, indexed by sets $\mathcal{T} = \{1, \dots, T\}$ and $\mathcal{U} = \{1, \dots, U\}$, respectively. The BS has K RF chains, where $K \leq U$. Each RF chain supports a single user's data stream. Following the current industry stance on ISAC, which advocates prioritizing communications while enabling sensing opportunistically, we predestine the use of RF chains primarily to serve user demands. Thus, users can be served individually or jointly with a target, but targets are not allocated RF chains for sensing only. The BS chooses J targets to sense from the total T , where $J \leq \min\{K, T\}$. In particular, each target is sensed simultaneously while servicing exactly one user¹. In the sequel, we denote the u -th user and the t -th target by U_u and T_t , respectively.

User scheduling: As the RF chains are limited, only a subset of users can be scheduled at a given channel use². Thus, we introduce constraints

$$\begin{aligned} C_1 : \mu_u &\in \{0, 1\}, \forall u \in \mathcal{U}, \\ C_2 : \sum_{u \in \mathcal{U}} \mu_u &= K. \end{aligned}$$

In C_1 , $\mu_u = 1$ indicates that U_u is scheduled, and $\mu_u = 0$ otherwise. Besides, C_2 enforces that all RF chains are used for communication, operating the system at maximum capacity.

¹To maintain a practical perspective and prevent performance degradation [13], we adopt a one-to-one pairing. Yet, our approach can be extended to a many-to-one pairing, allowing a user to be matched with multiple targets.

²We assume that unscheduled users are queued for a subsequent channel use, where resource allocation is re-executed to accommodate users who were not served in the current channel use, as well as any new arriving users requiring service.

Target scheduling: As the number of targets can be large, sensing all targets simultaneously is not feasible. To determine which targets are sensed in the current channel use, we add

$$\begin{aligned} C_3 : \lambda_t &\in \{0, 1\}, \forall t \in \mathcal{T}, \\ C_4 : \sum_{t \in \mathcal{T}} \lambda_t &= J. \end{aligned}$$

In C_3 , $\lambda_t = 1$ indicates that T_t is scheduled, and $\lambda_t = 0$ otherwise, while C_4 limits the scheduled targets to J .

User-target pairing: Some targets are paired with scheduled users, while others remain unpaired and unscheduled in the current channel use. To depict this, we add constraints

$$\begin{aligned} C_5 : \rho_{u,t} &\in \{0, 1\}, \forall u \in \mathcal{U}, t \in \mathcal{T}, \\ C_6 : \sum_{u \in \mathcal{U}} \rho_{u,t} &= \lambda_t, \forall t \in \mathcal{T}, \\ C_7 : \sum_{t \in \mathcal{T}} \rho_{u,t} &\leq \mu_u, \forall u \in \mathcal{U}. \end{aligned}$$

In C_5 , $\rho_{u,t} = 1$ indicates that U_u and T_t are paired, and $\rho_{u,t} = 0$ otherwise. Also, C_6 ensures that a scheduled target is paired with only one user, while C_7 restricts pairing to scheduled users only as sensing piggybacks on communications.

Communication model: The BS transmits signal $\mathbf{d} = \sum_{u \in \mathcal{U}} \mathbf{w}_u s_u$, where $\mathbf{w}_u \in \mathbb{C}^{N \times 1}$ is the beamforming vector for U_u , and $s_u \in \mathbb{C}$ is the data symbol for U_u , which follows a complex Gaussian distribution with zero mean and unit variance, e.g., $\mathbb{E}\{s_u s_u^*\} = 1$. The signal received by U_u is $y_u = \mathbf{h}_u^H \mathbf{d} + n_u = \sum_{u \in \mathcal{U}} \mathbf{h}_u^H \mathbf{w}_u s_u + n_u$, where $\mathbf{h}_u \in \mathbb{C}^{N \times 1}$ is the channel between the BS and U_u , and $n_u \sim \mathcal{CN}(0, \sigma^2)$ is additive white Gaussian noise (AWGN). The signal-to-interference-plus-noise ratio (SINR) of U_u is

$$\text{SINR}_u(\mathbf{W}) = |\tilde{\mathbf{h}}_u^H \mathbf{w}_u|^2 / (\sum_{i \in \mathcal{U}, i \neq u} |\tilde{\mathbf{h}}_u^H \mathbf{w}_i|^2 + 1), \quad (1)$$

where $\tilde{\mathbf{h}}_u = \frac{\mathbf{h}_u}{\sigma}$ and $\mathbf{W} = [\mathbf{w}_1, \dots, \mathbf{w}_U]$. Now, we add

$$C_8 : \begin{cases} \text{SINR}_u(\mathbf{W}) \geq \Gamma_{\text{th},u}, & \text{if } \mu_u = 1, \\ \text{SINR}_u(\mathbf{W}) = 0, & \text{if } \mu_u = 0 \end{cases}, \forall u \in \mathcal{U},$$

enforcing a SINR threshold $\Gamma_{\text{th},u}$ on scheduled users ($\mu_u = 1$) while not enforcing it on unscheduled users ($\mu_u = 0$).

Sensing model: The BS operates as a monostatic co-located radar, i.e., the angle of departure (AoD) and angle of arrival (AoA) are identical. The targets are modeled as single points, assuming they are far from the BS. The BS transmits signals in the directions of the targets, using the response matrices. The response matrix between the BS and T_t is $\mathbf{G}_t = \alpha_t \mathbf{a}(\theta_t) \mathbf{a}^H(\theta_t)$, $\forall t \in \mathcal{T}$, where α_t is the reflection coefficient of T_t [15], θ_t is the AoD/AoA of T_t , and $\mathbf{a}(\theta) = [e^{j\pi \frac{-N+1}{2} \cos(\theta)}, \dots, e^{j\pi \frac{N-1}{2} \cos(\theta)}]^T \in \mathbb{C}^{N \times 1}$ is the steering vector in the direction of θ , assuming half-wavelength antenna spacing. The directional power gain (DPG) is adopted as a design criterion for sensing [16], given by

$$\text{DPG}_t(\mathbf{v}_t) = \mathbf{v}_t^H \mathbf{G}_t \mathbf{v}_t, \forall t \in \mathcal{T}, \quad (2)$$

where \mathbf{v}_t is the beamforming vector used for illuminating T_t . Improving the DPG is crucial, as it increases the power radiated towards the targets, thereby enhancing detectability [16], [17]. Hence, we first introduce constraint

$$C_9 : \tau > 0,$$

where τ is an auxiliary variable, and then include constraint

$$C_{10} : \begin{cases} \mathbf{v}_t^H \mathbf{G}_t \mathbf{v}_t \geq \tau, & \text{if } \lambda_t = 1 \\ \mathbf{v}_t^H \mathbf{G}_t \mathbf{v}_t = 0, & \text{if } \lambda_t = 0 \end{cases}, \forall t, \in \mathcal{T},$$

to bound the DPG of the scheduled targets. We also add

$$C_{11} : \begin{cases} \mathbf{v}_t^H \mathbf{G}_q \mathbf{v}_t \leq \xi_{\text{th}}, & \text{if } \lambda_t = 1 \text{ and } \lambda_q = 1 \\ \mathbf{v}_t^H \mathbf{G}_q \mathbf{v}_t < \infty, & \text{otherwise} \end{cases}, \forall t, q \in \mathcal{T}, t \neq q,$$

to limit the cross-interference power among scheduled targets, where ξ_{th} is the maximum acceptable threshold [17].

Phase-only beamforming: The beamforming is designed with low-resolution constant-modulus discrete phases, given by set $\mathcal{S} = \{\delta e^{j\phi_1}, \dots, \delta e^{j\phi_L}\}$, where ϕ_l is the l -th phase, $\delta = \sqrt{\frac{P_{\text{tx}}}{KN}}$ is the magnitude, Q is the number of bits needed for representing the L phases in \mathcal{S} , and P_{tx} is the BS's transmit power. Thus, we include constraint

$$C_{12} : \begin{cases} [\mathbf{w}_u]_n \in \mathcal{S}, & \text{if } \mu_u = 1 \\ [\mathbf{w}_u]_n = 0, & \text{if } \mu_u = 0 \end{cases}, \forall u \in \mathcal{U}, n \in \mathcal{N},$$

which represents the beamforming design criteria for scheduled ($\mu_u = 1$) and unscheduled ($\mu_u = 0$) users. Since targets are paired and co-scheduled with users, then \mathbf{v}_t must be equal to one of the beamforming vectors \mathbf{w}_u , which is ensured by

$$C_{13} : \mathbf{v}_t = \sum_{u \in \mathcal{U}} \mathbf{w}_u \rho_{u,t}, \forall t \in \mathcal{T}.$$

Problem formulation: The joint user and target scheduling, user-target pairing, and low-resolution beamforming design is formulated by problem \mathcal{P} , whose objective is to maximize the minimum DPG of all scheduled targets via the use of τ .

$$\mathcal{P} : \underset{\Omega_{\mathcal{P}}}{\text{maximize}} \tau \text{ s.t. } C_1 - C_{13}.$$

Set $\Omega_{\mathcal{P}}$ encompasses all decision variables of \mathcal{P} , specifically, τ , μ_u , λ_t , $\rho_{u,t}$, \mathbf{w}_u , and \mathbf{v}_t . In particular, \mathcal{P} is a nonconvex MINLP, making it challenging to solve.

III. PROPOSED OPTIMAL APPROACH

We propose a series of equivalent transformations, detailed in Proposition 1 to Proposition 8, to reformulate the nonconvex MINLP \mathcal{P} into a convex, linear MILP \mathcal{Q} . This reformulation uncovers hidden convexities within \mathcal{P} , enabling its transformation into a tractable form without altering the original solution space. By preserving the original solution space at each step of the reformulation, we guarantee that an optimal solution to problem \mathcal{Q} is also optimal to problem \mathcal{P} . *The proofs for all subsequent propositions are provided in the Appendix.*

Proposition 1. *Constraint C_{12} can be equivalently rewritten as constraints D_1 , D_2 , and D_3 ,*

$$C_{12} \Leftrightarrow \begin{cases} D_1 : [\mathbf{x}_{u,n}]_l \in \{0, 1\}, \forall u \in \mathcal{U}, n \in \mathcal{N}, l \in \mathcal{L}, \\ D_2 : \mathbf{1}^T \mathbf{x}_{u,n} = \mu_u, \forall u \in \mathcal{U}, n \in \mathcal{N}, \\ D_3 : [\mathbf{w}_u]_n = \mathbf{s}^T \mathbf{x}_{u,n}, \forall u \in \mathcal{U}, n \in \mathcal{N}, \end{cases}$$

where vector $\mathbf{s} \in \mathbb{C}^{L \times 1}$ is formed by the elements in \mathcal{S} and $\mathcal{L} = \{1, \dots, L\}$.

Proposition 2. *Constraint C_8 can be equivalently rewritten as constraints E_1 and E_2 (at the top of next page), where $\tilde{\mathbf{H}}_u = \tilde{\mathbf{h}}_u \tilde{\mathbf{h}}_u^H$ and $B_{\text{max}} = P_{\text{tx}} \cdot \text{Tr}(\tilde{\mathbf{H}}_u) + 1$ is an upper bound for the left-hand-side (LHS) of E_2 .*

Proposition 3. *Constraint E_1 can be equivalently rewritten as constraint F_1 ,*

$$E_1 \Leftrightarrow F_1 : [\mathbf{W}_u]_{n,m} = [\mathbf{w}_u]_n [\mathbf{w}_u^*]_m, \forall u \in \mathcal{U}, n, m \in \mathcal{N},$$

where $[\mathbf{W}_u]_{n,m}$ represents the element of \mathbf{W}_u in the n -th row and m -th column.

Proposition 4. *Constraints D_3 and F_1 can be equivalently expressed as constraints G_1 , G_2 , and G_3 ,*

$$D_3 \Leftrightarrow \begin{cases} G_1 : [\mathbf{W}_u]_{n,m} = \text{Tr}(\mathbf{S} \mathbf{x}_{u,n} \mathbf{x}_{u,m}^T), \forall u \in \mathcal{U}, n \in \mathcal{N}, m \in \mathcal{M}_n, \\ G_2 : [\mathbf{W}_u]_{m,n} = [\mathbf{W}_u]_{n,m}^*, \forall u \in \mathcal{U}, n \in \mathcal{N}, m \in \mathcal{M}_n, \\ G_3 : [\mathbf{W}_u]_{n,n} = \delta^2 \mu_u, \forall u \in \mathcal{U}, n \in \mathcal{N}, \end{cases}$$

where $\mathbf{S} = \mathbf{s}^* \mathbf{s}^T$ and $\mathcal{M}_n = \{n+1, \dots, N\}$.

Proposition 5. *Constraint G_1 can be equivalently expressed as constraints H_1 , H_2 , and H_3 ,*

$$G_1 \Leftrightarrow \begin{cases} H_1 : \mathbf{Y}_{u,n,m} = \mathbf{x}_{u,n} \mathbf{x}_{u,m}^T, \forall u \in \mathcal{U}, n \in \mathcal{N}, m \in \mathcal{M}_n, \\ H_2 : [\mathbf{W}_u]_{n,m} = \text{Tr}(\mathbf{S} \mathbf{Y}_{u,n,m}), \forall u \in \mathcal{U}, n \in \mathcal{N}, m \in \mathcal{M}_n, \\ H_3 : [\mathbf{Y}_{u,n,m}]_{l,i} \in \{0, 1\}, \forall u \in \mathcal{U}, n \in \mathcal{N}, m \in \mathcal{M}_n, l, i \in \mathcal{L}, \end{cases}$$

Proposition 6. *Constraints H_1 and H_3 can be equivalently expressed as constraints I_1 , I_2 , and I_3 ,*

$$H_1 \Leftrightarrow \begin{cases} I_1 : \mathbf{1}^T [\mathbf{Y}_{u,n,m}]_{:,i} = [\mathbf{x}_{u,m}]_i, \forall u \in \mathcal{U}, n \in \mathcal{N}, m \in \mathcal{M}_n, i \in \mathcal{L}, \\ I_2 : [\mathbf{Y}_{u,n,m}]_{l,:} \mathbf{1} = [\mathbf{x}_{u,n}]_l, \forall u \in \mathcal{U}, n \in \mathcal{N}, m \in \mathcal{M}_n, l \in \mathcal{L}, \\ I_3 : [\mathbf{Y}_{u,n,m}]_{l,i} \in [0, 1], \forall u \in \mathcal{U}, n \in \mathcal{N}, m \in \mathcal{M}_n, l, i \in \mathcal{L}, \end{cases}$$

Proposition 7. *Constraint C_{10} is equivalent to constraint J_1 ,*

$$C_{10} \Leftrightarrow J_1 : \text{Tr}(\mathbf{G}_t \mathbf{W}_u) \geq \tau - (2 - \lambda_t - \rho_{u,t}) \bar{D}_t, \forall u \in \mathcal{U}, t \in \mathcal{T},$$

where $\bar{D}_t = \frac{P_{\text{tx}}}{K} \cdot \text{Tr}(\mathbf{G}_t)$.

Proposition 8. *Constraints C_{11} and C_{13} are equivalent to constraints K_1 , K_2 , K_3 , K_4 , and K_5 (at the top of next page).*

After applying the propositions above, nonconvex MINLP \mathcal{P} is equivalently recast as

$$\mathcal{Q} : \underset{\Omega_{\mathcal{Q}}}{\text{maximize}} \tau \\ \text{s.t.} \quad C_1, C_2, C_3, C_4, C_5, C_6, C_7, C_9, D_1, D_2, E_2, \\ G_2, G_3, H_2, I_1, I_2, I_3, J_1, K_1, K_2, K_3, K_4, K_5,$$

where $\Omega_{\mathcal{Q}}$ represents all decision variables of \mathcal{Q} , which include τ , μ_u , λ_t , $\rho_{u,t}$, $\pi_{t,q}$, \mathbf{w}_u , $\mathbf{x}_{u,n}$, \mathbf{W}_u , and $\mathbf{Y}_{u,n,m}$. In particular, \mathcal{Q} is an MILP, a convex optimization problem that can be solved to global optimality.

REMARK 1. *The worst-case computational complexity of \mathcal{P} is an exhaustive search (ES) requiring the evaluation of $\mathcal{C}_{\text{ES}} = 2^{KQN} \binom{U}{K} T!$ candidate solutions. Nevertheless, the special structure of \mathcal{Q} allows us to utilize branch-and-cut (BnC), implemented in commercial solvers, which can solve \mathcal{Q} optimally at a small fraction of \mathcal{C}_{ES} . In particular, BnC operates by pruning suboptimal and infeasible candidate solutions [18], which lies beyond the scope of this work.*

$$C_7 \Leftrightarrow \left\{ E_1 : \mathbf{W}_u = \mathbf{w}_u \mathbf{w}_u^H, \forall u \in \mathcal{U}, \quad E_2 : \sum_{i \in \mathcal{U}} \text{Tr}(\tilde{\mathbf{H}}_u \mathbf{W}_i) + 1 \leq (1 + \Gamma_{\text{th},u}^{-1}) \text{Tr}(\tilde{\mathbf{H}}_u \mathbf{W}_u) + (1 - \mu_u) \bar{B}_u, \forall u \in \mathcal{U}, \right.$$

$$C_{11}, C_{13} \Leftrightarrow \left\{ K_1 : \pi_{t,q} \leq \lambda_t, \forall t, q \in \mathcal{T}, t \neq q, \quad K_2 : \pi_{t,q} \leq \lambda_q, \forall t, q \in \mathcal{T}, t \neq q, \quad K_3 : \pi_{t,q} \geq \lambda_t + \lambda_q - 1, \forall t, q \in \mathcal{T}, t \neq q, \right. \\ \left. K_4 : \pi_{t,q} \in [0, 1], \forall t, q \in \mathcal{T}, t \neq q, \quad K_5 : \text{Tr}(\mathbf{G}_q \mathbf{W}_u) \leq \xi_{\text{th}} + (2 - \pi_{t,q} - \rho_{u,t}) \bar{D}_t, \forall u \in \mathcal{U}, t, q \in \mathcal{T}, t \neq q, \right.$$

IV. SIMULATION RESULTS

We evaluate our proposed approach using the Rician fading channel model. Thus, the channel for U_u is given by $\mathbf{h}_u = \gamma_u \mathbf{v}_u$, where γ_u accounts for large-scale fading and $\mathbf{v}_u = 1/\sqrt{K_R + 1} (\sqrt{K_R} \cdot \mathbf{v}_u^{\text{LoS}} + \mathbf{v}_u^{\text{NLoS}})$ is the normalized small-scale fading, with K_R denoting the fading factor. The line-of-sight (LoS) component is $\mathbf{v}_u^{\text{LoS}} = \mathbf{a}(\beta_u)$, where β_u is the LoS angle, and the non-LoS (NLoS) components are $\mathbf{v}_u^{\text{NLoS}} \sim \mathcal{CN}(\mathbf{0}, \mathbf{I})$. The LoS components are randomized but maintaining a separation of $\Delta = \beta_u - \beta_{u-1}$ between them to control the level of channel correlation. Here, $\gamma_u = 28 + 22 \log_{10}(d_u) + 20 \log_{10}(f_c) + \chi_u$ is computed using the UMA model [19], where f_c is the carrier frequency, $\chi_u \sim \mathcal{CN}(0, \zeta)$ is the shadowing for U_u , and d_u is the distance between the BS and U_u . We simulate 100 realizations considering deterministic parameters $K_R = 100$, $U = 5$, $K = 2$, $T = 4$, $J = 2$, $N = 12$ (cf. [20]), $\xi_{\text{th}} = 0.01$, $Q = 2$, $\mathcal{S} = \{\delta, j\delta, -\delta, -j\delta\}$, $f_c = 71$ GHz, $\sigma^2 = -87$ dBm, $\zeta = 4$ dB, and random parameters $\alpha_t \in [0.04, 0.08]$, $\theta_t \in [20, 160]$, and $d_u = [20, 80]$ m. We benchmark the following approaches, solved using CVX and MOSEK, with a tolerance of 0.01%, below which the solution is assumed to be optimal.

Optimal scheduling, pairing, and beamforming (OPT-SPB): This is the proposed approach, which yields an optimal design.

Baseline 1 (BL1): The pairing and scheduling are heuristic, while the beamforming is computed optimally as in **OPT-SPB**. This baseline prioritizes pairing over scheduling. Inspired by [13], the pairing is performed via bipartite graph matching (BGM), maximizing the sum of edge weights and yielding T user-target pairs. Each edge weight $\omega_{u,t} = \frac{|\mathbf{h}_u^H \mathbf{a}(\theta_t)|}{\|\mathbf{h}_u\| \|\mathbf{a}(\theta_t)\|}$ quantifies the alignment between U_u and T_t .

Baseline 2 (BL2): The pairing and scheduling are heuristic, while the beamforming is computed optimally as in **OPT-SPB**. This baseline prioritizes scheduling over pairing. Inspired by [13], [21], the scheduling involves choosing K users with the least mutual channel correlation. The correlation is defined as $\xi_{u,i} = \frac{|\mathbf{h}_u^H \mathbf{h}_i|}{\|\mathbf{h}_u\| \|\mathbf{h}_i\|}$ for any two users U_u and $U_i \neq u$. The pairing is done via BGM as in **BL1**, but using only the scheduled users.

Baseline 3 (BL3): Scheduling is random, choosing K users from U . Pairing and beamforming are optimal as in **OPT-SPB**.

Baseline 4 (BL4): Scheduling and pairing are performed randomly. The beamforming is optimal as in **OPT-SPB**.

Scenario I: We evaluate the impact of the transmit power on problem Q 's objective, i.e., τ , considering $\Gamma_{\text{th},u} = \Gamma_{\text{th}} = 4$, $\forall u \in \mathcal{U}$, and $\Delta = 10^\circ$. Fig. 2 shows that τ improves for all approaches as the transmit power increases, since the communication requirement remains invariant, leaving more power for sensing. In particular, **OPT-SPB** outperforms the baselines,

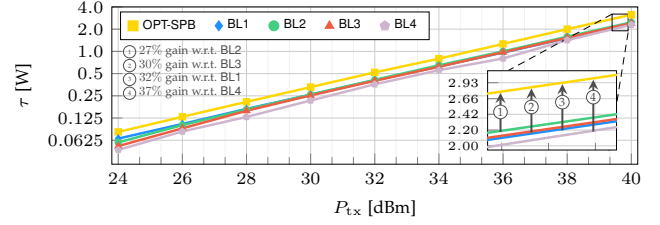


Fig. 2. Performance as a function of transmit power.

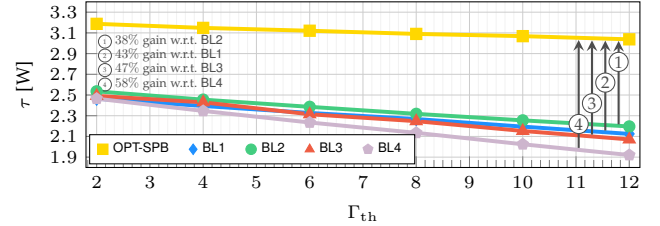


Fig. 3. Performance as a function of SINR threshold in correlated channels.

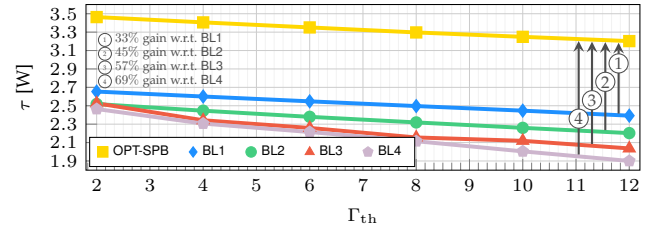


Fig. 4. Performance as a function of SINR threshold in uncorrelated channels.

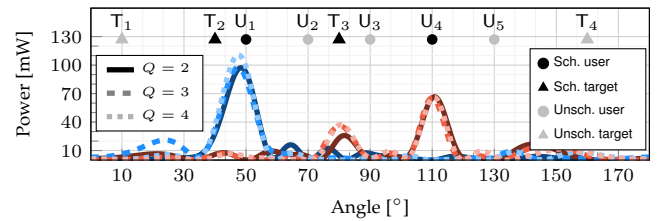


Fig. 5. Beampatterns for scheduled and paired users and targets.

achieving gains of over 27%, highlighting the importance of jointly designing scheduling, pairing, and beamforming, rather than addressing them separately as in the baselines. Among the baselines, **BL2** achieves the highest performance by scheduling users with the least correlated channels, effectively mitigating the high inter-user interference present in this scenario due to $\Delta = 10^\circ$. Although **BL3** ensures optimal pairing, **BL2** outperforms it. This highlights the crucial role of effective scheduling and demonstrates that simplistic scheduling, such as the random approach used in **BL3**, can significantly degrade performance. Additionally, **BL1** underperforms compared to **BL2**, despite its focus on maximizing alignment between users

and targets. This suggests that while alignment is beneficial, it is not the sole determinant of system performance and should be considered in conjunction with other factors, as demonstrated in *Scenario IV*. Lastly, **BL4** performs the worst, as its scheduling and pairing are random.

Scenario II: We evaluate the impact of the SINR threshold on sensing performance, considering $P_{\text{tx}} = 40$ dBm. Fig. 3 shows that τ decreases for all approaches as Γ_{th} increases, since the communication requirement becomes more stringent, leaving less power for sensing. **OPT-SPB** shows a significant advantage over the baselines, with gains exceeding 38% when $\Gamma_{\text{th}} = 12$. These results further emphasize the importance of joint design and highlight that meeting a stricter Γ_{th} becomes more challenging with suboptimal scheduling and pairing, leading to significant sensing performance degradation.

Scenario III: We consider the same parameters as in *Scenario II* but assume $\Delta = 30^\circ$. Fig. 4 shows that **OPT-SPB** outperforms the best baseline, **BL1** in this case, by 33%. This contrasts with previous scenarios where **BL2** was the best baseline. In those scenarios, users were spaced $\Delta = 10^\circ$ apart, leading to significant channel correlation, making user scheduling a critical factor. This favored **BL2**, whose user scheduling is designed to minimize correlation. However, in this scenario, users are spaced $\Delta = 30^\circ$, yielding lower channel correlation, thereby reducing the importance of user scheduling and shifting the focus to pairing. This explains why **BL1** now outperforms **BL2**, as it prioritizes pairing over scheduling, using alignment maximization. Moreover, Fig. 3 and Fig. 4 show that the performance of the baselines can vary significantly depending on the scenario characteristics, with certain settings favoring some schemes over others, while **OPT-SPB** performs consistently in all scenarios.

Scenario IV: Fig. 5 shows the beampatterns for a scenario, where $P_{\text{tx}} = 24$ dBm, $\Gamma_{\text{th}} = 12$, $U = 5$, $T = 4$, $K = J = 2$, $\beta_1 = 50$, $\beta_2 = 70$, $\beta_3 = 90$, $\beta_4 = 110$, $\beta_5 = 130$, $d_1 = d_3 = 60$ m, $d_2 = d_4 = d_5 = 80$ m, $\theta_1 = 10$, $\theta_2 = 40$, $\theta_3 = 80$, $\theta_4 = 160$, $\alpha_1 = 0.04$, $\alpha_2 = 0.08$, $\alpha_3 = 0.07$, and $\alpha_4 = 0.04$. Due to the high alignment between U_1 and T_2 , they are served by a broad beam. Besides, while U_2 and U_3 are also in close angular proximity to T_3 , their longer distances from the BS require more transmit power to serve them. Consequently, T_3 is paired with U_4 , even though they are not aligned, because U_4 is closer to the BS and requires less power, leaving more available for sensing T_3 . Here, U_4 is not paired with T_1 or T_4 because their lower reflection coefficients make them less favorable choices to maximize τ compared to T_3 . Also, three levels of phase resolution are considered: $Q = 2$, $Q = 3$, and $Q = 4$. Phase resolution plays a crucial role in improving the estimation of key parameters, such as AoA, which is frequently updated in applications like tracking. Specifically, the worst Cramér-Rao bound (CRB) of the AoAs for the given phase resolution levels are $56.002 \cdot 10^{-11}$, $24.191 \cdot 10^{-11}$, and $13.480 \cdot 10^{-11}$, respectively, demonstrating that higher phase resolution leads to smaller AoA estimation error. However, it is important to note that the CRB serves as an ideal lower bound and may not be achievable in practice, as it relies on the existence of an estimator that satisfies specific conditions. As such, these CRB values should be interpreted as theoretical benchmarks.

V. CONCLUSIONS

We investigated the joint design of scheduling, pairing, and beamforming, and proposed an approach that guarantees globally optimal solutions. We compared our approach to baselines relying on heuristic scheduling and pairing, and demonstrated that such methods can vary significantly in performance, underperforming compared to our approach. Our results highlight the importance of a holistic, integrated approach that effectively addresses all design aspects simultaneously.

APPENDIX

Proof of Proposition 1. We use binary variables to encode the phase selection for each element of the beamforming vector. A binary vector $\mathbf{x}_{u,n}$ is introduced for each U_u and antenna element n , as in D_1 . Phases are selected for U_u only if the user is scheduled, i.e., $\mu_u = 1$, which is enforced by D_2 . Finally, D_3 maps $\mathbf{x}_{u,n}$ to one of the phases in \mathbf{s} . ■

Proof of Proposition 2. For any U_u , the two cases in C_8 can be merged and equivalently recast as $\bar{Z}_a : \text{SINR}_u(\mathbf{w}) \geq \mu_u \cdot \Gamma_{\text{th},u}$. When $\mu_u = 1$, then \bar{Z}_a is equivalent to the first case. When $\mu_u = 0$, constraints D_2 and D_3 ensure $\mathbf{w}_u = \mathbf{0}$, making \bar{Z}_a collapse to the second case. Thus, constraint \bar{Z}_a can be rearranged as $\bar{Z}_b : (\sum_{i \in \mathcal{U}, i \neq u} |\tilde{\mathbf{h}}_u^H \mathbf{w}_i|^2 + 1)\mu_u \leq \Gamma_{\text{th},u}^{-1} |\tilde{\mathbf{h}}_u^H \mathbf{w}_u|^2$. Adding $|\tilde{\mathbf{h}}_u^H \mathbf{w}_u|^2$ to both sides of \bar{Z}_b leads to $\bar{Z}_c : (\sum_{i \in \mathcal{U}, i \neq u} |\tilde{\mathbf{h}}_u^H \mathbf{w}_i|^2 + 1)\mu_u + |\tilde{\mathbf{h}}_u^H \mathbf{w}_u|^2 \leq (1 + \Gamma_{\text{th},u}^{-1}) |\tilde{\mathbf{h}}_u^H \mathbf{w}_u|^2$. To get rid of the couplings between variables \mathbf{w}_i and μ_u , we apply the *big-M* method as in [10, p.8], equivalently transforming \bar{Z}_c into $\bar{Z}_d : \sum_{i \in \mathcal{U}} |\tilde{\mathbf{h}}_u^H \mathbf{w}_i|^2 + 1 \leq (1 + \Gamma_{\text{th},u}^{-1}) |\tilde{\mathbf{h}}_u^H \mathbf{w}_u|^2 + (1 - \mu_u) \bar{B}_u$, where \bar{B}_u is an upper bound of the LHS of \bar{Z}_d , computed via the trace inequality in Lemma 1. By introducing new variables $\mathbf{W}_u \in \mathbb{C}^{N \times N}$, $\forall u \in \mathcal{U}$, in constraint E_1 , we can recast constraint \bar{Z}_d as E_2 , where the cyclic property of the trace, in Lemma 2, was used, yielding $|\tilde{\mathbf{h}}_u^H \mathbf{w}_i|^2 = \text{Tr}(\mathbf{w}_i^H \tilde{\mathbf{h}}_u \tilde{\mathbf{h}}_u^H \mathbf{w}_i) = \text{Tr}(\mathbf{W}_i \tilde{\mathbf{H}}_u)$. ■

Proof of Proposition 3. Given $\mathbf{W}_u = \mathbf{w}_u \mathbf{w}_u^H$, the n -th row of \mathbf{W}_u is $[\mathbf{w}_u]_n \mathbf{w}_u^H$. In addition, the m -th element of the n -th row is $[\mathbf{w}_u]_n [\mathbf{w}_u^*]_m$. ■

Proof of Proposition 4. Replacing D_3 in F_1 results in $[\mathbf{W}_u]_{n,m} = \mathbf{s}^T \mathbf{x}_{u,n} \mathbf{x}_{u,m}^T \mathbf{s}^* = \text{Tr}(\mathbf{S} \mathbf{x}_{u,n} \mathbf{x}_{u,m}^T), \forall u \in \mathcal{U}, n, m \in \mathcal{N}$. Since \mathbf{W}_u is Hermitian, the elements of \mathbf{W}_u are conjugate symmetrical with respect to the diagonal, whereas all the diagonal elements are δ^2 when $\mu_u = 1$, and 0 when $\mu_u = 0$. Therefore, we only index the upper triangular part of \mathbf{W}_u resulting in G_1, G_2 , and G_3 . ■

Proof of Proposition 5. We introduce variable $\mathbf{Y}_{u,n,m} \in [0, 1]^{N \times N}$ to replace product $\mathbf{x}_{u,n} \mathbf{x}_{u,m}^T$, as stated in H_1 . Applying H_1 to G_1 leads to H_2 . In addition, $\mathbf{Y}_{u,n,m}$ is defined as having binary entries in H_3 to maintain the same nature of the product $\mathbf{x}_{u,n} \mathbf{x}_{u,m}^T$. ■

Proof of Proposition 6. For any scheduled user U_u , each of the vectors $\mathbf{x}_{u,n}$ and $\mathbf{x}_{u,m}^T$ have only one entry 1, according to D_2 . Based on H_1 , $\mathbf{Y}_{u,n,m}$ also has only one entry 1 while the remaining entries are 0. Specifically, if $[\mathbf{x}_{u,n}]_l = 1$

and $[\mathbf{x}_{u,m}]_i = 1$, then $[\mathbf{Y}_{u,n,m}]_{l,i} = 1$. We use this observation to eliminate the couplings $\mathbf{x}_{u,n}\mathbf{x}_{u,m}^T$. Due to space constraints, the following explanation solely focuses on the relation between \mathbf{H}_1 and \mathbf{I}_2 , given that \mathbf{I}_1 and \mathbf{I}_2 are similar in nature. Term $[\mathbf{x}_{u,n}]_l \mathbf{x}_{u,m}^T$ represents the l -th row of $\mathbf{Y}_{u,n,m}$, i.e., $[\mathbf{Y}_{u,n,m}]_{l,:} = [\mathbf{x}_{u,n}]_l \mathbf{x}_{u,m}^T$. When $[\mathbf{x}_{u,n}]_l = 0$, all the elements of $[\mathbf{Y}_{u,n,m}]_{l,:}$ are 0, meaning that the sum of all the elements of $[\mathbf{Y}_{u,n,m}]_{l,:}$ is $[\mathbf{x}_{u,n}]_l = 0$. When $[\mathbf{x}_{u,n}]_l = 1$, then $[\mathbf{Y}_{u,n,m}]_{l,:} = \mathbf{x}_{u,m}^T$. Given that $\mathbf{x}_{u,m}^T$ has only one entry equal to 1, then the sum of elements of $[\mathbf{Y}_{u,n,m}]_{l,:}$ must be $[\mathbf{x}_{u,n}]_l = 1$. Since $\mathbf{Y}_{u,n,m}$ has one entry 1, we can relax \mathbf{H}_3 such that $[\mathbf{Y}_{u,n,m}]_{l,i}$ is continuous in $[0, 1]$, which does not alter the solution space of $\mathbf{Y}_{u,n,m}$. In particular, this is ensured by the total unimodularity principle [22, ch.13], which allows recasting \mathbf{H}_3 and \mathbf{I}_3 , as long as \mathbf{I}_1 and \mathbf{I}_2 are included. ■

Proof of Proposition 7. By merging the two cases in \mathbf{C}_{10} and leveraging the cyclic property of the trace, in Lemma 2, \mathbf{C}_{10} can be expressed as constraint $\bar{\mathbf{Z}}_e : \text{Tr}(\mathbf{G}_t \mathbf{v}_t \mathbf{v}_t^H) \geq \tau \lambda_t$ for any target \mathbf{T}_t . While the first case in \mathbf{C}_{10} is directly implied by $\bar{\mathbf{Z}}_e$, the second case can be derived from \mathbf{C}_6 and \mathbf{C}_{13} , resulting in the equality to 0. Replacing \mathbf{v}_t , in \mathbf{C}_{13} , into $\bar{\mathbf{Z}}_e$ leads to $\bar{\mathbf{Z}}_f : \text{Tr}(\mathbf{G}_t (\sum_{u \in \mathcal{U}} \mathbf{w}_u \rho_{u,t}) (\sum_{i \in \mathcal{U}} \mathbf{w}_i \rho_{i,t})^H) \geq \tau \lambda_t$, eliminating the need for \mathbf{v}_t . Based on \mathbf{C}_6 and \mathbf{C}_7 , product $\rho_{u,t} \rho_{i,t}$ is 0 when $u \neq i$ because a target can only be paired with one user, thus leading us to defining $\bar{\mathbf{Z}}_f$ as $\bar{\mathbf{Z}}_g : \sum_{u \in \mathcal{U}} \text{Tr}(\mathbf{G}_t \mathbf{W}_u \rho_{u,t}) \geq \tau \lambda_t$, since $\rho_{u,t}^2 = \rho_{u,t}$. Constraint $\bar{\mathbf{Z}}_g$ exhibits two couplings, specifically, \mathbf{W}_u with $\rho_{u,t}$ and τ with λ_t , complicating the optimization of these variables. Leveraging \mathbf{C}_5 and applying the *big-M* method to $\bar{\mathbf{Z}}_g$, as in [10, p.8], we get rid of these multiplicative couplings, and thus express $\bar{\mathbf{Z}}_g$ equivalently as \mathbf{J}_1 , where $\bar{\mathbf{D}}_t$ is an upper bound of the LHS of $\bar{\mathbf{Z}}_g$, computed via Lemma 1. ■

Proof of Proposition 8. The procedure follows a similar approach to Proposition 7. Note that the first case of \mathbf{C}_{11} is only active when $\lambda_t = \lambda_q = 1$, while the second case is always satisfied due to the limited transmit power. Therefore, instead of using ∞ in the second case, we can substitute it with the upper bound $\bar{\mathbf{D}}_t$, derived in Proposition 7. Thus, for any target \mathbf{T}_t , this allows us to combine the two cases of \mathbf{C}_{11} into a single case, resulting in $\bar{\mathbf{Z}}_h : \mathbf{v}_t^H \mathbf{G}_q \mathbf{v}_t \leq \xi_{\text{th}} + (1 - \lambda_t \lambda_q) \bar{\mathbf{D}}_t$. The LHS of $\bar{\mathbf{Z}}_h$ is similar to the LHS of $\bar{\mathbf{Z}}_e$, thus we can recast $\bar{\mathbf{Z}}_h$ as $\bar{\mathbf{Z}}_i : \sum_{u \in \mathcal{U}} \text{Tr}(\mathbf{G}_q \mathbf{W}_u \rho_{u,t}) \leq \xi_{\text{th}} + (1 - \lambda_t \lambda_q) \bar{\mathbf{D}}_t$. This constraint can be split into $\bar{\mathbf{Z}}_{i_1} : \pi_{t,q} = \lambda_t \lambda_q$ and $\bar{\mathbf{Z}}_{i_2} : \sum_{u \in \mathcal{U}} \text{Tr}(\mathbf{G}_q \mathbf{W}_u \rho_{u,t}) \leq \xi_{\text{th}} + (1 - \pi_{t,q}) \bar{\mathbf{D}}_t$. Leveraging Lemma 3, $\bar{\mathbf{Z}}_{i_1}$ can be expressed as $\mathbf{K}_1, \mathbf{K}_2, \mathbf{K}_3$, and \mathbf{K}_4 , while $\bar{\mathbf{Z}}_{i_2}$ is equivalently recast as \mathbf{K}_5 using the *big-M* method as in Proposition 7. ■

Lemma 1. [23, p.2] Given positive semidefinite matrices \mathbf{A} and \mathbf{B} , the following holds $\text{Tr}(\mathbf{AB}) \leq \text{Tr}(\mathbf{A}) \text{Tr}(\mathbf{B})$.

Lemma 2. Given matrices $\mathbf{A}, \mathbf{B}, \mathbf{C}$, and \mathbf{D} of compatible dimensions, the following holds $\text{Tr}(\mathbf{ABCD}) = \text{Tr}(\mathbf{BCDA})$.

Lemma 3. Let $c = ab$, where $a, b \in \{0, 1\}$. Thus, this equality is equivalent to the intersection of $\mathbf{R}_1 : c \leq a, \mathbf{R}_2 : c \leq b, \mathbf{R}_3 : c \geq a + b - 1$, and $\mathbf{R}_4 : c \in [0, 1]$.

REFERENCES

- [1] F. Liu, C. Masouros, A. P. Petropulu, H. Griffiths, and L. Hanzo, "Joint radar and communication design: Applications, state-of-the-art, and the road ahead," *IEEE Trans. Commun.*, vol. 68, no. 6, pp. 3834–3862, 2020.
- [2] T. Mao, J. Chen, Q. Wang, C. Han, Z. Wang, and G. K. Karagiannidis, "Waveform design for joint sensing and communications in millimeter-wave and low terahertz bands," *IEEE Trans. Commun.*, vol. 70, no. 10, pp. 7023–7039, 2022.
- [3] S. Dutta, C. N. Barati, D. Ramirez, A. Dhananjay, J. F. Buckwalter, and S. Rangan, "A case for digital beamforming at mmWave," *IEEE Trans. Wireless Commun.*, vol. 19, no. 2, pp. 756–770, 2020.
- [4] W. Lyu, S. Yang, Y. Xiu, Y. Li, H. He, C. Yuen, and Z. Zhang, "CRB minimization for RIS-aided mmWave integrated sensing and communications," *IEEE Internet Things J.*, vol. 11, no. 10, pp. 18381–18393, 2024.
- [5] A. Kaushik, A. Arora, C. Tsinos, C. Masouros, F. Liu, and S. Chatzinothas, "Waveform design for joint radar-communications with low complexity analog components," in *Proc. of IEEE JC&S*, 2022, pp. 1–5.
- [6] C. G. Tsinos, A. Arora, S. Chatzinothas, and B. Ottersten, "Dual-function radar-communication systems with constant-modulus and similarity constraints," in *Proc. of IEEE SAM*, 2022, pp. 231–235.
- [7] Z. Xiao, S. Chen, and Y. Zeng, "Simultaneous multi-beam sweeping for mmWave massive MIMO integrated sensing and communication," *IEEE Trans. Veh. Technol.*, vol. 73, no. 6, pp. 8141–8152, 2024.
- [8] N. Su, F. Liu, C. Masouros, T. Ratnarajah, and A. Petropulu, "Secure dual-functional radar-communication transmission: Hardware-efficient design," in *Proc. of ACSSC*, 2021, pp. 629–633.
- [9] X. Wang, Z. Fei, J. Huang, and H. Yu, "Joint waveform and discrete phase shift design for RIS-assisted integrated sensing and communication system under Cramer-Rao bound constraint," *IEEE Transactions on Vehicular Technology*, vol. 71, no. 1, pp. 1004–1009, 2022.
- [10] L. F. Abanto-Leon, A. Asadi, A. Garcia-Saavedra, G. H. Sim, and M. Hollick, "RadiOrchestra: Proactive management of millimeter-wave self-backhauled small cells via joint optimization of beamforming, user association, rate selection, and admission control," *IEEE Trans. Wireless Commun.*, vol. 22, no. 1, pp. 153–173, 2023.
- [11] C. Dou, N. Huang, Y. Wu, L. Qian, and T. Q. S. Quek, "Sensing-efficient NOMA-aided integrated sensing and communication: A joint sensing scheduling and beamforming optimization," *IEEE Trans. Veh. Technol.*, vol. 72, no. 10, pp. 13591–13603, 2023.
- [12] N. Zhao, Y. Wang, Z. Zhang, Q. Chang, and Y. Shen, "Joint transmit and receive beamforming design for integrated sensing and communication," *IEEE Commun. Lett.*, vol. 26, no. 3, pp. 662–666, 2022.
- [13] C. Dou, N. Huang, Y. Wu, L. Qian, and T. Q. S. Quek, "Channel sharing aided integrated sensing and communication: An energy-efficient sensing scheduling approach," *IEEE Trans. Wireless Commun.*, vol. 23, no. 5, pp. 4802–4814, 2024.
- [14] L. Cazzella, M. Mizmizi, D. Tagliaferri, D. Badini, M. Matteucci, and U. Spagnolini, "Deep learning-based target-to-user association in integrated sensing and communication systems," 2024. [Online]. Available: <https://arxiv.org/abs/2401.12801>
- [15] J. Li and P. Stoica, "MIMO radar with colocated antennas," *IEEE Signal Process. Mag.*, vol. 24, no. 5, pp. 106–114, 2007.
- [16] J. Li, G. Zhou, T. Gong, and N. Liu, "Beamforming design for active IRS-aided MIMO integrated sensing and communication systems," *IEEE Wireless Commun. Lett.*, vol. 12, no. 10, pp. 1786–1790, 2023.
- [17] K. Meng, Q. Wu, R. Schober, and W. Chen, "Intelligent reflecting surface enabled multi-target sensing," *IEEE Transactions on Communications*, vol. 70, no. 12, pp. 8313–8330, 2022.
- [18] J. Desrosiers and M. Lübbecke, "Branch-price-and-cut algorithms," in *Wiley Encyclopedia of Operations Research and Management Science*, 2010.
- [19] 3GPP, "Study on channel model for frequencies from 0.5 to 100 GHz," 3rd Generation Partnership Project (3GPP), Technical Report (TR) 38.901, 2020, version 16.1.0.
- [20] SiBEAM SK62xx-MOD transceiver module, SiBEAM. [Online]. Available: <https://fcc.report/FCC-ID/UK2MOD621X/3593226.pdf>
- [21] D. Christopoulos, S. Chatzinothas, and B. Ottersten, "Multicast multi-group precoding and user scheduling for frame-based satellite communications," *IEEE Trans. Wireless Commun.*, vol. 14, no. 9, pp. 4695–4707, 2015.
- [22] C. H. Papadimitriou and K. Steiglitz, *Combinatorial optimization: Algorithms and complexity*. Courier Corporation, 1998.
- [23] Z. Yang and X. Feng, "A note on the trace inequality for products of Hermitian matrix power," *J. Inequal. Pure Appl. Math.*, vol. 3, no. 5, pp. 1–12, 2002.